Models for Bearing Damage Detection in Induction Motors Using Stator Current Monitoring

Martin Blödt, Pierre Granjon, Bertrand Raison, Gilles Rostaing

Models for Bearing Damage Detection in Induction Motors Using Stator Current Monitoring

Martin Blödt, *Member, IEEE*, Pierre Granjon, Bertrand Raison, *Member, IEEE*, and Gilles Rostaing

***Abstract*—This paper describes a new analytical model for the influence of rolling-element bearing faults on induction motor stator current. Bearing problems are one major cause for drive failures. Their detection is possible by vibration monitoring of characteristic bearing frequencies. As it is possible to detect other machine faults by monitoring the stator current, a great interest exists in applying the same method for bearing fault detection. After a presentation of the existing fault model, a new detailed approach is proposed. It is based on the following two effects of a bearing fault: 1) the introduction of a particular radial rotor movement and 2) load torque variations caused by the bearing fault. The theoretical study results in new expressions for the stator current frequency content. Experimental tests with artificial and realistic bearing damage were conducted by measuring vibration, torque, and stator current. The obtained results by spectral analysis of the measured quantities validate the proposed theoretical approach.**

***Index Terms*—Airgap eccentricity, bearing damage detection, induction motors, motor current signature analysis, spectral analysis, torque variations.**

I. Introduction

INDUCTION motors are nowadays widely used in all types of industry applications due to their simple construction, high reliability, and the availability of power converters using efficient control strategies. A permanent condition monitoring of the electrical drive can further increase the productivity, reliability, and safety of the entire installation.

Traditionally, motor condition can be supervised by measuring quantities such as noise, vibration, and temperature. The implementation of these measuring systems is expensive and proves only to be rentable in the case of large motors or critical applications. A solution to this problem can be the use of quantities that are already measured in a drive system, e.g., the machine's stator current, which is often required for command purposes. A general review of monitoring and fault diagnosis techniques can be found in [1]–[5].

The different faults that may occur in an electrical machine can be classified as follows [6]:

- stator faults, e.g., short circuit, loss of supply phase;
- rotor faults, e.g., broken bar, broken end-ring;
- static and dynamic eccentricities;
- bearing faults.

Bearing faults are the most frequent faults in electric motors (41%) according to an IEEE motor reliability study for large motors above 200 hp [7], followed by stator (37%) and rotor faults (10%). Schoen *et al.* [8] have proposed a model for bearing fault detection based on the generation of fault-related rotating eccentricities. This fault model has been applied in several recent works [2], [9]–[12].

In this paper, a more detailed approach will be introduced, taking also into account fault-related torque variations. First, a short overview of bearing fault types is given in Section II, followed by the characteristic vibration frequencies and the existing fault model developed by Schoen. In Sections III and IV, the theoretical background for a new model is developed and new expressions for the frequency content of the stator current in case of bearing faults are obtained. Section V gives a short summary and discussion of the theoretical results. Experimental results with different fault types are given in Section VI, validating different aspects of the theoretical approach. This paper has been previously published in a shortened form in the Proceedings of the IEEE International Symposium on Industrial Electronics 2004 [13].

II. Existing Models for Bearing Fault Detection

A. Bearing Fault Types

This paper considers rolling-element bearings with a geometry shown in Fig. 1. The bearing consists mainly of the outer and inner raceways, the balls, and the cage, which assures equidistance between the balls. The number of balls is denoted N_b, their diameter is D_b, and the pitch or cage diameter is D_c. The point of contact between a ball and the raceway is characterized by the contact angle β.

Bearing faults can be categorized into distributed and localized defects [14], [15]. Distributed defects affect a whole region and are difficult to characterize by distinct frequencies. In contrast, single-point defects are localized and can be classified according to the following affected element:

- outer raceway defect;
- inner raceway defect;
- ball defect.

Manuscript received July 17, 2006; revised November 12, 2007. This work was supported by Schneider Electric S.A. This work was partly presented at the IEEE International Symposium on Industrial Electronics, Ajaccio, France, May 4–7, 2004.

M. Blödt was with the Laboratoire d'Electrotechnique de Grenoble, 38402 Grenoble, France and with Schneider Electric S.A., F-92500 Rueil-Malmaison, France. He is now with Siemens AG, 80333 Munich, Germany (e-mail: Martin.Bloedt@siemens.com).

P. Granjon is with the Gipsa-Laboratory, Institut National Polytechnique de Grenoble, 38031 Grenoble, France (e-mail: pierre.granjon@gipsa-lab.fr).

B. Raison and G. Rostaing are with the Laboratoire de Génie Electrique de Grenoble, Institut National Polytechnique de Grenoble, 38402 Saint Martin d'Hères, France (e-mail: bertrand.raison@g2elab.inpg.fr; gilles.rostaing@g2elab.inpg.fr).

Color versions of one or more of the figures in this paper are available online at http://ieeexplore.ieee.org.

Digital Object Identifier 10.1109/TIE.2008.917108

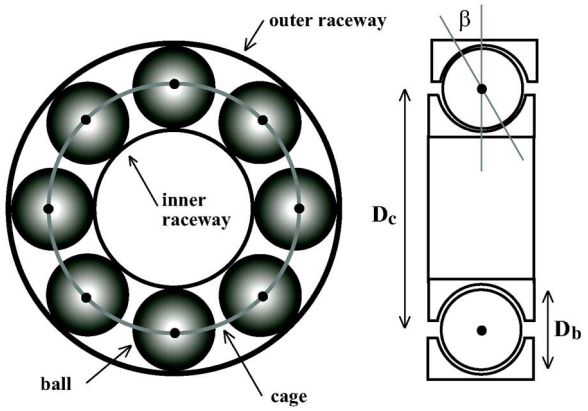

Fig. 1. Geometry of a rolling-element bearing.

A single-point defect could be imagined as a small hole, a pit, or a missing piece of material on the corresponding element. Only those will be considered in the following.

Some publications [3], [6] consider an additional fault type, the cage fault. However, it will not be discussed in this paper.

B. Characteristic Frequencies

With each type of bearing fault, a characteristic frequency f_c can be associated. This frequency is equivalent to the periodicity by which an anomaly appears due to the existence of the fault. Imagining for example a hole on the outer raceway: as the rolling elements move over the defect, they are regularly in contact with the hole, which produces an effect on the machine at a given frequency.

The characteristic frequencies are functions of the bearing geometry and the mechanical rotor frequency f_r. A detailed calculation of these frequencies can be found in [16]. For the three considered fault types, f_c takes the following expressions:

$$\text{Outer raceway}: \quad f_0 = \frac{N_b}{2} f_r \left(1 - \frac{D_b}{D_c}\cos\beta\right) \tag{1}$$

$$\text{Inner raceway}: \quad f_i = \frac{N_b}{2} f_r \left(1 + \frac{D_b}{D_c}\cos\beta\right) \tag{2}$$

$$\text{Ball}: \quad f_b = \frac{D_c}{D_b} f_r \left(1 - \frac{D_b^2}{D_c^2}\cos^2\beta\right). \tag{3}$$

It has been statistically shown in [17] that the vibration frequencies can be approximated for most bearings with between 6 and 12 balls by

$$f_0 = 0.4\, N_b f_r \tag{4}$$

$$f_i = 0.6\, N_b f_r. \tag{5}$$

Vibration measurement is traditionally used to detect bearing defects. Analytical models describing the vibration response of bearing with single-point defects can be found in [14], [18], and [19].

C. Bearing Fault Detection by Stator Current Analysis

The most often quoted model studying the influence of bearing damage on the induction machine's stator current was proposed by Schoen *et al.* [8]. The authors consider the generation of rotating eccentricities at bearing fault characteristic frequencies f_c, which leads to periodical changes in the machine inductances. This should produce additional frequencies $f_{\rm bf}$ in the stator current, which is given by

$$f_{\rm bf} = |f_s \pm k f_c| \tag{6}$$

where f_s is the electrical stator supply frequency, and $k = 1, 2, 3, \ldots$.

This model has been applied in a large amount of different works. In [11] and [12], time–frequency methods based on Schoen's model are used to identify bearing faults by analyzing stator current. Stack *et al.* [15] examine single-point defects and generalized roughness. Schoen's model components are also analyzed by using parametric [20] and nonparametric [2], [9] spectral analysis, neural networks, and/or wavelet transform [10], [21].

We consider this model to be incomplete: On the one hand, no detailed theoretical development of the fault-related frequency expression is given. On the other hand, it does not consider torque variations as a consequence of the bearing fault. In Sections III and IV, the simple existing model for bearing fault consequences on the stator current will be completed and extended by the means of a more detailed theoretical study.

III. Theoretical Study I: Radial Rotor Movement

The following two physical effects are considered in the theoretical study when the defect comes into contact with another bearing element:

1) the introduction of a radial movement of the rotor center;
2) the apparition of load torque variations.

The method used to study the influence of the rotor displacement on the stator current is based on the magnetomotive force (MMF) and permeance wave approach, which is traditionally used when considering static and dynamic eccentricities or rotor and stator slotting [22]–[24]. To the author's knowledge, it has not been applied to the analysis of bearing faults yet. The first step is the calculation of the airgap permeance Λ, which is closely related to the airgap length g. The magnetic field in the airgap can then be determined by multiplying the permeance waves by the rotor and stator MMFs. Finally, the stator current can be obtained from the magnetic field by the stator voltage equations of the induction machine.

The following model is based on several simplifying assumptions. First, load zone effects in the bearing are not considered. The fault impact on the airgap length is considered by a series of Dirac generalized functions. In reality, the fault generates other pulse shapes, but this alters only the harmonic amplitudes. Since this modeling approach focuses on the frequency combinations and modulation types and not on exact amplitudes, this assumption is reasonable. In the second part of load torque oscillations, the higher order terms of the load torque Fourier series are neglected since higher frequencies in the rotor speed and angle are considerably dampened due to the mechanical equation. The calculation of the airgap magnetic field does not take into account higher order space and time harmonics for the

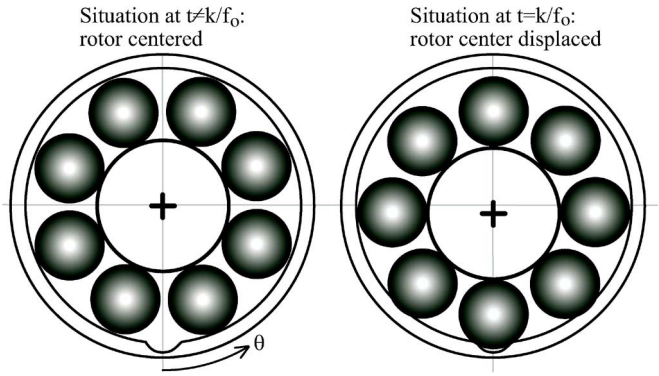

Fig. 2. Radial rotor movement due to an outer bearing raceway defect.

sake of simplicity. However, the calculated modulation effects affect higher harmonics in the same way as the fundamental.

The additional fault-related stator current components produce themselves rotating stator fields that may generate additional rotor fields and torque components. These higher order armature reactions are difficult to take into account with a simple analytical model. Moreover, they will be of relatively small amplitude and are therefore neglected in these simplified considerations.

A. Airgap Length Variations

The first step in the theoretical analysis is the determination of the airgap length g as a function of time t and angular position θ in the stator reference frame. The radial rotor movement causes the airgap length to vary as a function of the defect, which is always considered as a hole or a point of missing material in the corresponding bearing element.

1) Outer Race Defect: Without loss of generality, the outer race defect can be assumed to be located at the angular position $\theta = 0$. When there is no contact between a ball and the defect, the rotor is perfectly centered. In this case, the airgap length g is supposed to take the constant value g_0, neglecting rotor and stator slotting effects. On the contrary, every $t = k/f_0$ (with k integer), the contact between a ball and the defect leads to a small movement of the rotor center in the stator reference frame (see Fig. 2). In this case, the airgap length can be approximated by $g_0(1 - e_0 \cos\theta)$, where e_0 is the relative degree of eccentricity [25]. In order to model the fault impact on the airgap length as a function of time, a series of Dirac generalized functions can then be used, as it is common in models for vibration analysis [18].

These considerations lead to the following expression for the airgap length:

$$g_0(\theta, t) = g_0 \left[1 - e_0 \cos(\theta) \sum_{k=-\infty}^{+\infty} \delta \left(t - \frac{k}{f_0} \right) \right] \quad (7)$$

where e_0 is the relative degree of eccentricity introduced by the outer race defect. This equation can be interpreted as a temporary static eccentricity of the rotor, appearing only at $t = k/f_0$. The function $g_0(\theta, t)$ is represented in Fig. 3 for $\theta = 0$ as an example.

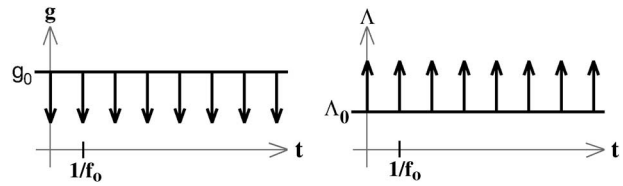

Fig. 3. Airgap length g and permeance Λ in the presence of an outer bearing raceway defect for $\theta = 0$.

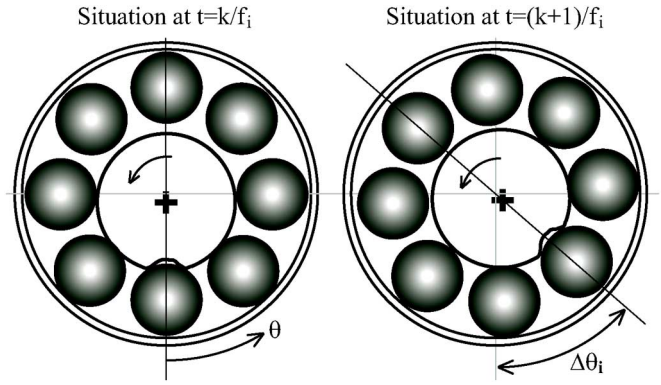

Fig. 4. Radial rotor movement due to an inner bearing raceway defect.

2) Inner Race Defect: In this case, the situation is slightly different from the outer race defect. The fault occurs at the instants $t = k/f_i$. As the defect is located on the inner race, the angular position of the minimal airgap length moves with respect to the stator reference frame as the rotor turns at the angular frequency ω_r (see Fig. 4). Between two contacts with the defect, the defect itself has moved by an angle described by

$$\Delta\theta_i = \omega_r \Delta t = \frac{\omega_r}{f_i}. \quad (8)$$

Hence, (7) becomes

$$g_i(\theta, t) = g_0 \left[1 - e_i \sum_{k=-\infty}^{+\infty} \cos(\theta + k\Delta\theta_i) \delta \left(t - \frac{k}{f_i} \right) \right] \quad (9)$$

where e_i is the relative degree of eccentricity introduced by the inner race defect.

This equation can be simplified for further calculations by extracting the cosine term of the sum, so that the series of Dirac generalized functions may be later developed into a Fourier series. One fundamental property of the Dirac generalized function is given by the following equation [26]:

$$h(k) \cdot \delta \left(t - \frac{k}{f_i} \right) = h(tf_i) \cdot \delta \left(t - \frac{k}{f_i} \right). \quad (10)$$

This formula becomes obvious when one considers that $\delta(t - k/f_i)$ is always equal to 0, except for $t = k/f_i$. After combining (8)–(10), the airgap length becomes

$$g_i(\theta, t) = g_0 \left[1 - e_i \cos(\theta + \omega_r t) \sum_{k=-\infty}^{+\infty} \delta \left(t - \frac{k}{f_i} \right) \right]. \quad (11)$$

3) Ball Defect: In the presence of a ball defect, the defect location moves in a similar way as the inner raceway fault. The fault causes an anomaly on the airgap length at the instants $t = k/f_b$. The angular position of minimal airgap length changes as a function of the cage rotational frequency. The balls are all fixed in the cage that rotates at the fundamental cage frequency ω_{cage}, which is given by [16]

$$\omega_{\text{cage}} = \frac{1}{2}\omega_r \left(1 - \frac{D_b}{D_c}\cos\beta\right). \tag{12}$$

The angle $\Delta\theta_b$ by which the fault location has moved between two fault impacts becomes

$$\Delta\theta_b = \omega_{\text{cage}}\Delta t = \frac{\omega_{\text{cage}}}{f_b}. \tag{13}$$

By analogy with (11), the expression of airgap length in the presence of a ball defect becomes

$$g_b(\theta, t) = g_0 \left[1 - e_b \cos(\theta + \omega_{\text{cage}} t) \sum_{k=-\infty}^{+\infty} \delta\left(t - \frac{k}{f_b}\right)\right] \tag{14}$$

where e_b is the relative degree of eccentricity introduced by the ball defect.

4) Generalization: In order to simplify the following considerations, (7), (11), and (14) can be combined in a generalized expression for the airgap length g in the presence of a bearing fault, i.e.,

$$g(\theta, t) = g_0 \left[1 - e\,\cos(\theta + \psi(t)) \sum_{k=-\infty}^{+\infty} \delta\left(t - \frac{k}{f_c}\right)\right] \tag{15}$$

where f_c is the characteristic bearing fault frequency given by (1), (2), or (3), and $\psi(t)$ is defined as follows:

$$\psi(t) = \begin{cases} 0 & \text{for an outer race defect} \\ \omega_r t & \text{for an inner race defect} \\ \omega_{\text{cage}} t & \text{for a ball defect.} \end{cases} \tag{16}$$

B. Airgap Permeance

The airgap permeance Λ is proportional to the inverse of the airgap length g and is defined as follows:

$$\Lambda = \frac{\mu}{g} \tag{17}$$

where $\mu = \mu_r \mu_0$ is the magnetic permeability of the airgap. In the case of a bearing fault, with (15), the permeance becomes

$$\Lambda(\theta, t) = \Lambda_0 \frac{1}{\left[1 - e\,\cos(\theta + \psi(t)) \sum\limits_{k=-\infty}^{+\infty} \delta\left(t - \frac{k}{f_c}\right)\right]} \tag{18}$$

where $\Lambda_0 = \mu/g_0$. The relationship between airgap length $g(\theta, t)$ and airgap permeance $\Lambda(\theta, t)$ is illustrated in Fig. 3 at the position $\theta = 0$ for an outer raceway defect.

First, in order to simplify this expression, the fraction $1/(1-x)$ is approximated for small airgap variations by the first-order term of its series development, i.e.,

$$\begin{aligned} \frac{1}{1-x} &= 1 + x + x^2 + x^3 + \cdots, \qquad \text{for } |x| < 1 \\ &\approx 1 + x. \end{aligned} \tag{19}$$

The condition $|x| < 1$ is always satisfied because the degree of eccentricity verifies $|e| < 1$ in order to avoid contact between the rotor and the stator.

Second, the series of Dirac generalized functions is expressed as a complex Fourier series development [18], [26], i.e.,

$$\begin{aligned} \sum_{k=-\infty}^{+\infty} \delta\left(t - \frac{k}{f_c}\right) &= \sum_{k=-\infty}^{+\infty} c_k e^{-\mathrm{j}2\pi k f_c t} \\ &= c_0 + 2\sum_{k=1}^{+\infty} c_k \cos(2\pi k f_c t) \end{aligned} \tag{20}$$

with the Fourier series coefficients $c_k = f_c \forall k$.

Equations (18)–(20) can be combined into a simplified expression for the airgap permeance wave, i.e.,

$$\begin{aligned} \Lambda(\theta, t) \approx \Lambda_0 \Bigg\{ & 1 + e c_0 \cos(\theta + \psi(t)) \\ & + e \sum_{k=1}^{+\infty} c_k \cos(\theta + \psi(t) + k\omega_c t) \\ & + e \sum_{k=1}^{+\infty} c_k \cos(\theta + \psi(t) - k\omega_c t) \Bigg\}. \end{aligned} \tag{21}$$

C. Airgap Flux Density

The flux density in the airgap is determined by multiplying the MMF with the permeance wave. For the sake of clarity and to demonstrate the modulation effects, only the fundamental MMF waves are considered, i.e., space and time harmonics are neglected. However, they should theoretically be subject to the same modulation effects as the fundamental. Rotor and stator fundamental MMFs are waves at supply frequency $\omega_s = 2\pi f_s$ with p pole pairs (where p is the pole pair number of the machine). The total MMF F_{tot} is given by their sum and is assumed as

$$F_{\text{tot}}(\theta, t) = F\,\cos(p\theta - \omega_s t + \varphi). \tag{22}$$

Multiplication of (21) and (22) leads to the following expression of the flux density distribution:

$$\begin{aligned} B_{\text{tot}}(\theta, t) &= F_{\text{tot}}(\theta, t) \cdot \Lambda(\theta, t) \\ &= F\Lambda_0 \cos(p\theta - \omega_s t + \varphi) \\ &\quad + \sum_{k=0}^{\infty} B_k [\cos\,((p \pm 1)\theta \pm \psi(t) \pm k\omega_c t - \omega_s t + \varphi)] \end{aligned} \tag{23}$$

where B_k are the amplitudes of the fault-related flux density waves. The notation $\pm$ is used to write all possible frequency combinations in a compact form.

Equation (23) clearly shows the influence of the rotor displacement caused by the bearing fault on the flux density: In addition to the fundamental sine wave (term B_0), a multitude of fault-related sine waves appear in the airgap. These supplementary waves have $p \pm 1$ pole pairs and a frequency content f_{ecc} that is given by

$$f_{\text{ecc}} = \frac{1}{2\pi}\left(\pm\frac{d\psi(t)}{dt} \pm k\omega_c - \omega_s\right). \tag{24}$$

D. Stator Current

The additional flux density components according to (23) are equivalent to an additional magnetic flux $\Phi(\theta, t)$. By considering the realization of the winding and the geometry of the machine, the additional flux $\Phi(t)$ in each stator phase can be obtained. If the stator voltages are imposed, the time-varying flux causes additional components in the machine's stator current according to the following stator voltage equation for phase m:

$$V_m(t) = R_s I_m(t) + \frac{d\Phi_m(t)}{dt}. \tag{25}$$

The frequency content of the flux in each phase is supposed to be equal to the frequency content of the airgap field according to (24). Under the hypothesis of imposed stator voltages, the stator current in each phase is given by the derivative of the corresponding flux. This leads to the following expression for the stator current $I_m(t)$ with ω_r assumed constant:

$$I_m(t) = \sum_{k=0}^{\infty} I_k \cos\left[\pm\psi(t) \pm k\omega_c t - \omega_s t + \varphi_m\right]. \tag{26}$$

Thus, it becomes obvious that the radial rotor movement due to the bearing fault results in additional frequencies in the stator current. With the three fault types, the following frequencies are obtained from (16) and (26):

$$\text{Outer race defect :} \quad f_{\text{ecc or}} = f_s \pm k f_0 \tag{27}$$

$$\text{Inner race defect :} \quad f_{\text{ecc ir}} = f_s \pm f_r \pm k f_i \tag{28}$$

$$\text{Ball defect :} \quad f_{\text{ecc ball}} = f_s \pm f_{\text{cage}} \pm k f_b \tag{29}$$

where $k = 1, 2, 3, \ldots$. These expressions have never been mentioned in former publications.

In terms of signal processing, it can be noticed that the effect of the fault-related rotor movement on the stator current is an amplitude modulation of the fundamental sine wave, due to the effect of the modified permeance on the fundamental MMF wave.

In the previous calculation of the magnetic airgap field, only the fundamental MMF has been considered. Bearing in mind the existence of time harmonics in the MMF, the same additional frequencies will appear not only around the fundamental frequency f_s but also around higher supply frequency harmonics and even around the rotor slot harmonics.

IV. Theoretical Study II: Torque Variations

In this section, the second considered effect of a bearing fault on the machine is studied. Imagining for example a hole in the outer race: each time a ball passes in a hole, a mechanical resistance will appear when the ball tries to leave the hole. The consequence is a small increase of the load torque at each contact between the defect and another bearing element. The bearing fault-related torque variations appear at the previously mentioned characteristic vibration frequencies f_c (see Section II-B) as they are both of the same origin: a contact between the defect and another element.

Load torque variations have been studied, e.g., by Salles *et al.* [27] or Legowski *et al.* [28]. However, they always considered stator current amplitude modulation as a consequence of the periodically varying load torque. Section IV-A provides a more detailed analysis and demonstrates that, on the contrary, the stator current is phase modulated.

A. Effect on Rotor MMF

Under a bearing fault, the load torque as a function of time can be described by a constant component Γ_0 and an additional component varying at the characteristic frequency f_c. The first term of the variable component's Fourier series development is a cosine varying at frequency f_c. For the sake of clarity, higher order terms are neglected in the following and only the fundamental term is considered. The load torque can therefore be described by

$$\Gamma_{\text{load}}(t) = \Gamma_0 + \Gamma_c \cos(\omega_c t) \tag{30}$$

where Γ_c is the amplitude of the bearing fault-related torque variations, and $\omega_c = 2\pi f_c$.

The application of the mechanical equation of the machine leads to the influence of the torque variations on motor speed ω_r, i.e.,

$$\sum \Gamma(t) = \Gamma_{\text{motor}}(t) - \Gamma_{\text{load}}(t) = J\frac{d\omega_r}{dt}$$
$$\Leftrightarrow \omega_r(t) = \frac{1}{J}\int_t \left(\Gamma_{\text{motor}}(\tau) - \Gamma_{\text{load}}(\tau)\right) d\tau \tag{31}$$

where Γ_{motor} is the electromagnetic torque produced by the machine, and J is the total inertia of the system machine load.

In steady-state, the motor torque is assumed to be equal to the constant part of the load torque, i.e., $\Gamma_{\text{motor}}(t) = \Gamma_0$. This leads to

$$\omega_r(t) = -\frac{1}{J}\int_{t_0}^{t} \Gamma_c \cos(\omega_c \tau) d\tau + C$$
$$= -\frac{\Gamma_c}{J\omega_c}\sin(\omega_c t) + \omega_{r0}. \tag{32}$$

The mechanical speed consists, therefore, of a constant component ω_{r0} and a sinusoidally varying one.

The next step is the calculation of the mechanical rotor position θ_r, which is the integral of the mechanical speed, i.e.,

$$\theta_r(t) = \int_{t_0}^{t} \omega_r(\tau)d\tau = \frac{\Gamma_c}{J\omega_c^2}\cos(\omega_c t) + \omega_{r0}t. \quad (33)$$

The integration constant has been assumed to be equal to zero. In contrast to the healthy machine where $\theta_r(t) = \omega_{r0}t$, variations at the characteristic frequencies are present on the mechanical rotor position.

The variations of the mechanical rotor position θ_r have an influence on the rotor MMF. In a normal state, the rotor MMF in the rotor reference frame R is a wave with p pole pairs and a frequency sf_s and is given by

$$F_r^{(R)}(\theta, t) = F_r \cos\left(p\theta' - s\omega_s t\right) \quad (34)$$

where θ' is the mechanical angle in the rotor reference frame, and s is the motor slip.

The transformation between the rotor and stator reference frames is defined by $\theta = \theta' + \theta_r$. Using (33), this leads to

$$\theta' = \theta - \omega_{r0}t - A_c \cos\left(\omega_c t\right) \quad (35)$$

where $A_c = \Gamma_c/(J\omega_c^2)$ is the amplitude of the angle variations.

Thus, the rotor MMF given in (34) can be transformed to the stationary stator reference frame using (35) and $\omega_{r0} = \omega_s(1 - s)/p$, i.e.,

$$F_r(\theta, t) = F_r \cos\left(p\theta - \omega_s t - pA_c \cos\left(\omega_c t\right)\right). \quad (36)$$

It becomes clear from this expression that the torque variations at frequency f_c lead to a phase modulation of the rotor MMF in the stator reference frame. This phase modulation is characterized by the introduction of the term $pA_c \cos\left(\omega_c t\right)$ in the phase of the MMF wave.

B. Effect on Flux Density and Stator Current

The airgap flux density B is the product of total MMF and permeance. First, the airgap length and the resulting permeance are assumed constant. The additional fault-related flux density components are obtained by considering the interaction between the modified rotor MMF and the permeance. This leads to

$$B(\theta, t) = F_{r,1}\Lambda_0 \cos\left(p\theta - \omega_s t - pA_c \cos\left(\omega_c t\right)\right). \quad (37)$$

The phase modulation present on the flux density can be consecutively found on the flux in a machine phase. Considering (25), the stator current in phase m is given by the derivation of the flux, leading to the following expression:

$$\begin{aligned} I_m(t) = {} & I_1 \sin\left(\omega_s t + pA_c \cos\left(\omega_c t\right)\right) \\ & + I_2 \sin\left(\omega_s t + pA_c \cos\left(\omega_c t\right) + \omega_c t\right) \\ & - I_2 \sin\left(\omega_s t + pA_c \cos\left(\omega_c t\right) - \omega_c t\right). \end{aligned} \quad (38)$$

The term I_1 keeps the initial phase modulation found on the rotor MMF; the expressions with I_2 result from the derivation and should be of smaller amplitude than the term I_1.

TABLE I
SUMMARY OF BEARING FAULT-RELATED FREQUENCIES IN THE STATOR CURRENT SPECTRUM

	according to Schoen [8]	according to the present approach	
		Eccentricity	Torque variations
Outer raceway	$f_s \pm kf_o$	$f_s \pm kf_o$	$f_s \pm kf_o$
Inner raceway	$f_s \pm kf_i$	$f_s \pm f_r \pm kf_i$	$f_s \pm kf_i$
Ball defect	$f_s \pm kf_b$	$f_s \pm f_{cage} \pm kf_b$	$f_s \pm kf_b$

As the frequency content of a signal $x(t) = A\cos\varphi(t)$ is given by the time derivative of its phase $\varphi(t)$ (in terms of instantaneous frequency, see [29]), the frequency of the fault-related components in the stator current is given by

$$f(t) = \frac{1}{2\pi}\frac{d\varphi(t)}{dt} = f_s - pA_c f_c \sin(\omega_c t) \pm kf_c \quad (39)$$

where $k = 0$ or 1. The effects of the fault-related torque variations on the motor current are therefore phase modulations, which are equivalent to a time-varying frequency content.

As in Section III, the time harmonics of rotor MMF and the nonuniform airgap permeance have not been considered. However, the harmonics of supply frequency f_s and the rotor slot harmonics will theoretically show the same phase modulations as the fundamental component.

V. SUMMARY

The frequencies found in the preceding theoretical study enlarge the existing model of the effects of bearing faults on stator current but also stand in contrast to it. Schoen *et al.* [8] considered only one effect of the fault: the introduction of a radial rotor movement. The theoretical model in this paper considers the following two effects: 1) the radial rotor movement and 2) torque variations.

Considering the radial rotor movement, the obtained formulas give the same result as the existing model only in the case of an outer raceway defect. The other fault types lead to different expressions [see (27)–(29)], involving frequencies such as the shaft rotational frequency or the bearing cage frequency.

The torque variations principally lead to phase modulations at f_c of the stator current fundamental frequency f_s, i.e., a time-varying frequency content. The phase modulations produce a characteristic signature on the power spectral density (PSD), which is given by sideband components around the fundamental at $f_s \pm kf_c$, where $k = 1, 2, 3, \ldots$ [30]. Although Schoen *et al.* [8] did not consider torque variations as a consequence of bearing faults, these produce the same signature on the current spectrum as given in (6). Table I summarizes the fault-related frequencies in the stator current spectrum and compares them to those proposed by Schoen *et al.*

VI. EXPERIMENTAL RESULTS

A. Test Rig

The experimental tests were carried out on a test rig with a standard 1.1-kW two-pole pair Y-coupled induction motor. A direct current machine was used to simulate different load

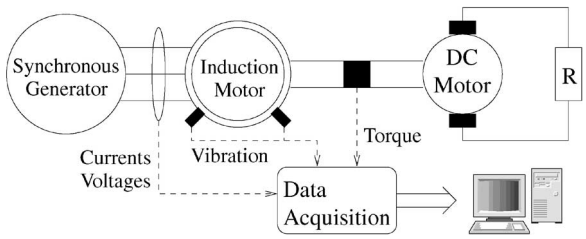

Fig. 5. Scheme of the experimental setup.

Fig. 6. Photo of bearings with single-point defects. (a) Outer raceway defect. (b) Inner raceway defect.

levels. In order to reduce the harmonic content in the supply voltage, the induction motor is directly fed by a synchronous generator (100 kVA). Measured quantities are the three line currents, the stator voltages, motor speed, torque, and two vibration signals issued from piezoelectric accelerometers mounted on the stator core. Data are sampled at 16 kHz and processed using Matlab. The test rig is schematically displayed in Fig. 5.

Two classes of faulty bearings (NSK 6205) are available. First, new bearings have been artificially damaged to produce defects on the outer and inner raceways. The defects consist of holes that have been drilled axially through the raceways (see Fig. 6). Second, bearings with realistic damage, which are issued from industrial maintenance, were tested. The faulty bearings are mounted at the load end of the induction machine.

The characteristic vibration frequencies take the following values at no-load operation: outer raceway frequency $f_0 = 89.6$ Hz, inner raceway frequency $f_i = 135.4$ Hz, and ball frequency $f_b = 58.8$ Hz. The contact angle β has been assumed to be zero.

B. Outer Raceway Defect

The defect on the outer raceway has already been experimentally studied in [8], so that it will be discussed very shortly. During the tests, the characteristic vibration frequency and its multiples were clearly visible on the vibration spectrum of the machine. There also appeared torque variations at the characteristic vibration frequencies.

The current spectrum shows a characteristic component at 125 Hz, which corresponds to the frequency combination $|f_s - 2f_0|$ (see Fig. 7). It is interesting to note that the same frequency combination appeared in [31], where a bearing with an outer race defect was experimentally tested.

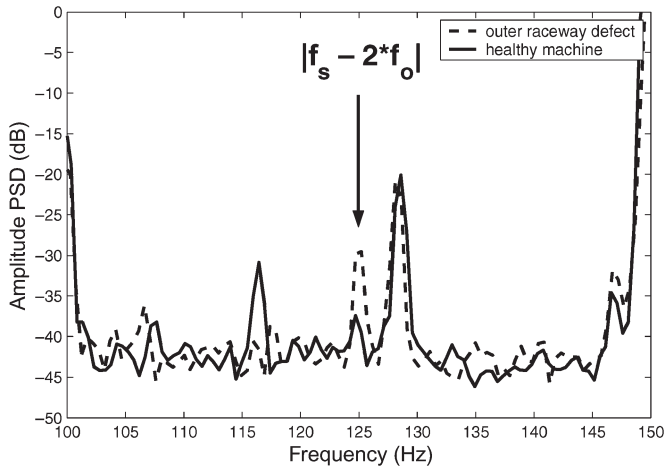

Fig. 7. Stator current spectrum of the loaded machine with outer raceway defect.

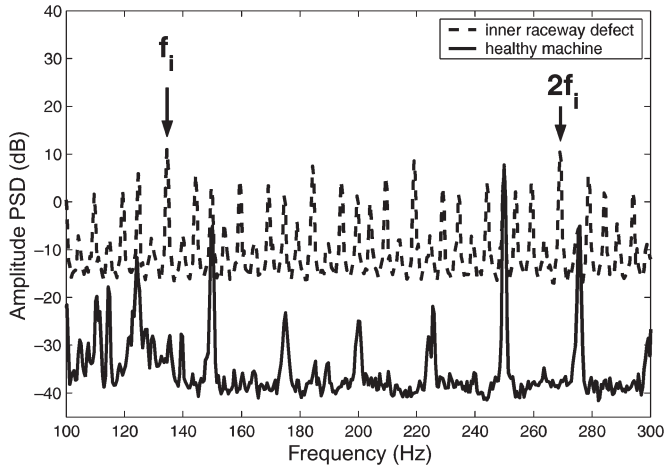

Fig. 8. Vibration spectrum of the unloaded machine with inner raceway defect.

C. Inner Raceway Defect

In a first step, the vibration signal is analyzed. A logarithmic plot of the vibration spectrum with a damaged bearing in comparison with the healthy machine condition is shown in Fig. 8. The characteristic frequencies of the inner raceway defect f_i and its multiples (e.g., $2f_i$) are the components with the largest magnitude. Multiple tests with different load levels permitted to observe slight variations of the characteristic vibration frequency according to (2). Additional components due to other mechanical effects, e.g., the cage rotational frequency ($\approx$10 Hz) and a general rise of the vibration level can also be noticed on the vibration spectrum.

A spectral analysis of the measured load torque is shown in Fig. 9. The characteristic fault frequency f_i clearly appears on the torque spectrum with an amplitude of +15 dB in comparison to the healthy case. This validates the proposed theoretical approach, which assumes torque variations at the characteristic frequency as a consequence of the bearing fault. Higher harmonics of f_i can also be observed. In addition to the aforementioned components, other frequencies appear in

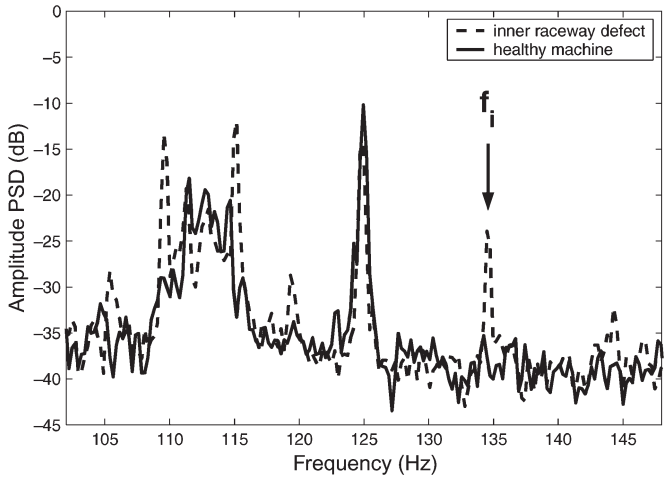

Fig. 9. Torque spectrum of the unloaded machine with inner raceway defect.

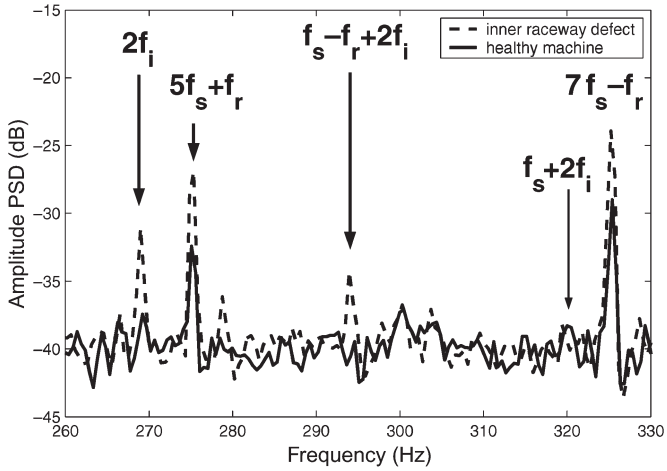

Fig. 10. Stator current spectrum of the unloaded machine with inner raceway defect.

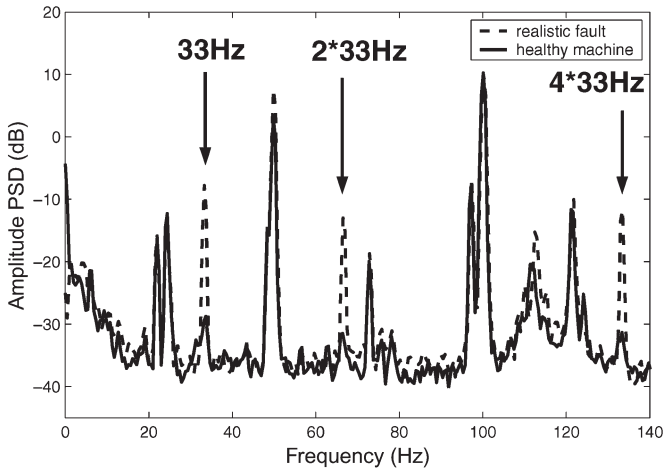

Fig. 11. Torque spectrum of the loaded machine with realistic bearing fault.

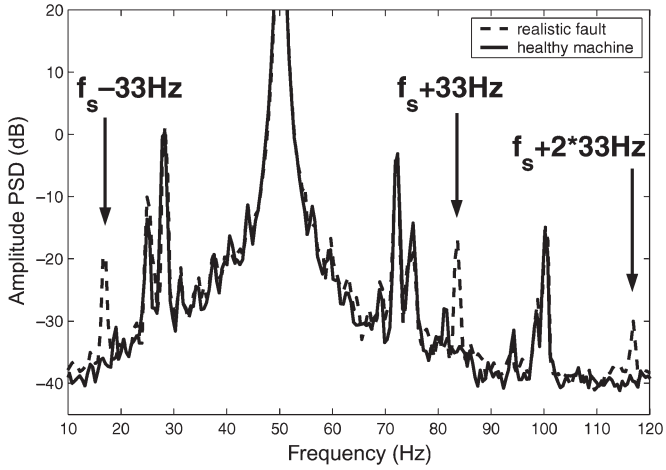

Fig. 12. Stator current spectrum of the loaded machine with realistic bearing fault.

the torque spectrum at, e.g., 110 and 115 Hz, but they have no direct link to a predicted characteristic frequency.

The stator current spectrum (see Fig. 10) shows, on the one hand, a rise of eccentricity related components. The frequency components at $5f_s + f_r$ and $7f_s - f_r$ are already present in the spectrum of the healthy machine due to an inherent level of dynamic eccentricity. The fault-related eccentricity increases these components according to (28) (with $k = 0$). The component at $f_s - f_r + 2f_i$ does not appear in the healthy spectrum but in case of the fault, as it is the consequence of the particular form of eccentricity introduced by the inner raceway fault. Another fault-related component at $2f_i$ can be noticed. On the contrary, no particular rise in amplitude can be noticed at $f_s + 2f_i$ where it should be according to the expressions mentioned by Schoen *et al.* [8]. The obtained results for this fault validate, therefore, the precedent theoretical development.

D. Realistic Bearing Fault

After the so-called "artificial" bearing faults, tests were conducted with industrially used bearings that have been changed due to a problem with an unknown fault type. The tested bearing shows only small effects on the vibration spectrum, such as a small peak at 33 Hz and a slight general increase of the vibration level for frequencies higher than 150 Hz. Characteristic vibration frequencies could not have been clearly identified.

However, the measured machine torque shows considerable changes in comparison to the healthy case (see Fig. 11). At nominal load level, torque variations of great amplitude can be identified at 33 Hz and its multiples.

These torque variations have a considerable effect on the stator current. In Fig. 12, the stator current spectrum with the faulty bearing can be compared to the healthy machine. Sideband components to the fundamental appear at $50 \pm k \cdot 33$ Hz. This is the characteristic signature on the spectrum of a phase modulation of the fundamental component (see [30]).

As a phase modulation is equivalent to a time-varying frequency of the analytic signal [see (39)], time–frequency methods can be used to verify the theoretical prediction that torque variations create a phase modulation on the stator current. Time–frequency methods [32] are used in signal processing applications when nonstationary signals are analyzed.

One basic method is to compute the instantaneous frequency [29] of a signal. The idea is to use the Hilbert transform to obtain a complex form of the original real signal called analytic

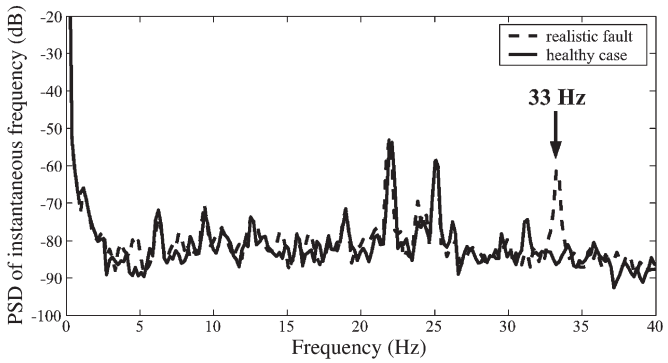

Fig. 13. Stator current instantaneous frequency spectrum of the loaded machine with realistic bearing fault.

signal. The phase information of a complex can easily be retrieved considering its argument. The instantaneous frequency of the signal is then obtained by the derivation of the phase [see (39)]. This definition of instantaneous frequency is only valid for a signal having one single component.

However, the measured stator current on the test rig naturally contains a multitude of harmonic components so that the instantaneous frequency cannot be directly computed on the signal. The following steps are necessary in order to obtain useful information.

1) The stator current is low-pass filtered at approximately two times the fundamental frequency.
2) The current signal is downsampled to a sampling rate at about four times the fundamental frequency in order to reduce the data volume.
3) The Hilbert transform is used on the real current signal in order to obtain the analytic signal.
4) The instantaneous frequency of the fundamental component is calculated using the Matlab Time–Frequency Toolbox [33].

In Fig. 13, the PSD of the instantaneous frequency is shown for the healthy and faulty cases. The significant difference is a component at 33 Hz in the faulty case. The spectral peak at this frequency indicates variations at 33 Hz of the fundamental stator current component. These variations are a sign of phase modulations present in the faulty case. Considering the measured torque variations with the faulty bearing (see Fig. 11), it can be concluded that the observed phase modulation is the consequence of the recognized torque variations, as it has been developed in Section IV.

E. Summary of Experimental Results

The previous experimental results have validated several theoretical aspects. The produced single-point defects showed the expected effects on the vibration spectrum, i.e., the apparition of the characteristic vibration frequencies. In case of inner and outer race faults, the measured load torque showed variations at these frequencies, confirming that the assumption of bearing fault-related torque oscillations is valid. Furthermore, significant effects could be observed in the stator current spectrum, i.e., the apparition of some of the theoretically predicted frequencies.

Moreover, low-frequency load torque oscillations have been observed with a realistic bearing fault. The resulting stator current shows phase modulations, which validates the second part of the theoretical study.

However, it must be noted that the amplitudes of the additional stator current frequencies may depend heavily on the considered bearing and the load condition. Therefore, a systematic bearing monitoring using only the stator current is difficult to realize. Nevertheless, in some cases, the stator current showed more significant effects than the vibration data, which suggests that a combined approach using vibration and current analysis could be reasonable.

VII. Conclusion

This paper has investigated the detection of rolling-element bearing faults in induction motors by stator current monitoring. A new fault model has been proposed, which considers fault-related airgap length variations and changes in the load torque. The theoretical development is based on airgap field calculation by MMF and permeance wave approach. New expressions for the frequency content of the stator current are obtained for the three major fault types.

An experimental study has been conducted on a test rig with several faulty bearings, measuring quantities such as machine vibrations, torque, and stator current. The spectral analysis shows that characteristic vibration frequencies are visible in the torque spectrum. The torque oscillations lead to changes in the stator current spectrum. Other fault-related components are due to a particular fault-related radial rotor movement.

In order to validate the hypothesis of phase modulations in the stator current as a consequence of torque variations, a basic time–frequency method, the instantaneous frequency, has been applied. The result proves that the torque oscillations lead indeed to a time-varying frequency content, which corroborates the predicted phase modulations.

It has therefore been shown that bearing faults can cause significant changes in the stator current spectrum that can be used for fault diagnosis purposes.

Acknowledgment

The authors would like to thank C.-S. Maroni of Schneider Electric for her support and C. Brun for having produced the bearing faults.

References

[1] D. Basak, A. Tiwari, and S. P. Das, "Fault diagnosis and condition monitoring of electrical machines—A review," in *Proc. IEEE ICIT*, Mumbai, India, Dec. 2006, pp. 3061–3066.
[2] J. H. Jung, J. J. Lee, and B. H. Kwon, "Online diagnosis of induction motors using MCSA," *IEEE Trans. Ind. Electron.*, vol. 53, no. 6, pp. 1842–1852, Dec. 2006.
[3] S. Nandi and H. A. Toliyat, "Condition monitoring and fault diagnosis of electrical machines—A review," in *Conf. Rec. IAS Annu. Meeting*, Phoenix, AZ, Oct. 1999, vol. 1, pp. 197–204.
[4] M. E. H. Benbouzid, "A review of induction motors signature analysis as a medium for faults detection," *IEEE Trans. Ind. Electron.*, vol. 47, no. 5, pp. 984–993, Oct. 2000.
[5] M. E. H. Benbouzid and G. B. Kliman, "What stator current processing-based technique to use for induction motor rotor faults diagnosis?" *IEEE Trans. Energy Convers.*, vol. 18, no. 2, pp. 238–244, Jun. 2003.

[6] P. Vas, *Parameter Estimation, Condition Monitoring and Diagnosis of Electrical Machines*. Oxford, U.K.: Clarendon, 1993.
[7] IEEE Motor Reliability Working Group, "Report of large motor reliability survey of industrial and commercial installations," *IEEE Trans. Ind. Appl.*, vol. IA-21, no. 4, pp. 853–872, Jul. 1986.
[8] R. R. Schoen, T. G. Habetler, F. Kamran, and R. Bartheld, "Motor bearing damage detection using stator current monitoring," *IEEE Trans. Ind. Appl.*, vol. 31, no. 6, pp. 1274–1279, Nov./Dec. 1995.
[9] L. Sun and B. Xu, "An improvement of stator current based detection of bearing fault in induction motors," in *Conf. Rec. IAS Annu. Meeting*, Tampa, FL, Oct. 2007, pp. 2277–2281.
[10] L. Eren, K. Teotrakool, and M. J. Devaney, "Bearing fault detection via wavelet packet decomposition with spectral post processing," in *Proc. IEEE Instrum. Meas. Technol. Conf.*, Warsaw, Poland, May 2007, pp. 1–4.
[11] A. Lebaroud and G. Clerc, "Time–frequency classification applied to induction machine faults monitoring," in *Proc. 32nd Annu. Conf. IEEE IECON*, Paris, France, Nov. 2006, pp. 5051–5056.
[12] B. Yazici and G. B. Kliman, "An adaptive statistical time–frequency method for detection of broken bars and bearing faults in motors using stator current," *IEEE Trans. Ind. Appl.*, vol. 35, no. 2, pp. 442–452, Mar./Apr. 1999.
[13] M. Blödt, P. Granjon, B. Raison, and G. Rostaing, "Models for bearing damage detection in induction motors using stator current monitoring," in *Proc. IEEE ISIE*, Ajaccio, France, May 2004, pp. 383–388.
[14] N. Tandon and A. Choudhury, "An analytical model for the prediction of the vibration response of rolling element bearings due to a localized defect," *J. Sound Vib.*, vol. 205, no. 3, pp. 275–292, Aug. 1997.
[15] J. Stack, T. G. Habetler, and R. G. Harley, "Fault classification and fault signature production for rolling element bearings in electric machines," *IEEE Trans. Ind. Appl.*, vol. 40, no. 3, pp. 735–739, May/Jun. 2004.
[16] B. Li, M. Chow, Y. Tipsuwan, and J. Hung, "Neural-network-based motor rolling bearing fault diagnosis," *IEEE Trans. Ind. Electron.*, vol. 47, no. 5, pp. 1060–1069, Oct. 2000.
[17] R. L. Schiltz, "Forcing frequency identification of rolling element bearings," *Sound Vib.*, vol. 24, no. 5, pp. 16–19, May 1990.
[18] P. D. MacFadden and J. D. Smith, "Model for the vibration produced by a single point defect in a rolling element bearing," *J. Sound Vib.*, vol. 96, no. 1, pp. 69–82, Sep. 1984.
[19] Y. F. Wang and P. J. Kootsookos, "Modeling of low shaft speed bearing faults for condition monitoring," *Mech. Syst. Signal Process.*, vol. 12, no. 3, pp. 415–426, May 1998.
[20] J. Stack, T. G. Habetler, and R. G. Harley, "Bearing fault detection via autoregressive stator current modeling," *IEEE Trans. Ind. Appl.*, vol. 40, no. 3, pp. 740–747, May/Jun. 2004.
[21] L. Eren, A. Karahoca, and M. J. Devaney, "Neural network based motor bearing fault detection," in *Proc. IMTC*, Como, Italy, May 2004, vol. 3, pp. 1657–1660.
[22] J. R. Cameron and W. T. Thomson, "Vibration and current monitoring for detecting airgap eccentricity in large induction motors," *Proc. Inst. Electr. Eng.*, vol. 133, no. 3, pp. 155–163, May 1986.
[23] D. G. Dorrell, W. T. Thomson, and S. Roach, "Analysis of airgap flux, current, and vibration signals as a function of the combination of static and dynamic airgap eccentricity in 3-phase induction motors," *IEEE Trans. Ind. Appl.*, vol. 33, no. 1, pp. 24–34, Jan./Feb. 1997.
[24] S. Nandi, S. Ahmed, and H. A. Toliyat, "Detection of rotor slot and other eccentricity related harmonics in a three phase induction motor with different rotor cages," *IEEE Trans. Energy Convers.*, vol. 16, no. 3, pp. 253–260, Sep. 2001.
[25] H. Guldemir, "Detection of airgap eccentricity using line current spectrum of induction motors," *Electr. Power Syst. Res.*, vol. 64, no. 2, pp. 109–117, Feb. 2003.
[26] J. Max and J.-L. Lacoume, *Méthodes et Techniques de Traitement du Signal*, 5th ed. Paris, France: Dunod, 2000.
[27] G. Salles, F. Filippetti, C. Tassoni, G. Grellet, and G. Franceschini, "Monitoring of induction motor load by neural network techniques," *IEEE Trans. Power Electron.*, vol. 15, no. 4, pp. 762–768, Jul. 2000.
[28] S. F. Legowski, A. H. M. S. Ula, and A. M. Trzynadlowski, "Instantaneous power as a medium for the signature analysis of induction motors," *IEEE Trans. Ind. Appl.*, vol. 32, no. 4, pp. 904–909, Jul./Aug. 1996.
[29] B. Boashash, "Estimating and interpreting the instantaneous frequency of a signal—Part 1: Fundamentals," *Proc. IEEE*, vol. 80, no. 4, pp. 520–538, Apr. 1992.
[30] A. B. Carlson, *Communication Systems: An Introduction to Signals and Noise in Electrical Communication*, 3rd ed. New York: McGraw-Hill, 1986.
[31] E. L. Bonaldi, L. E. B. da Silva, G. Lambert-Torres, L. E. L. Oliveira, and F. O. Assuncao, "Using rough sets techniques as a fault diagnosis classifier for induction motors," in *Proc. IEEE IECON*, Sevilla, Spain, Nov. 2002, vol. 4, pp. 3383–3388.
[32] P. Flandrin, *Time–Frequency/Time-Scale Analysis*. San Diego, CA: Academic, 1999.
[33] F. Auger, P. Flandrin, P. Gonçalvès, and O. Lemoine, *Time–Frequency Toolbox*. France: CNRS/Rice Univ., 1995–1996. [Online]. Available: http://tftb.nongnu.org

Martin Blödt (S'04–M'06) was born in Baden-Baden, Germany, in 1978. He received the double diploma degree in electrical engineering from the University of Karlsruhe (TH), Karlsruhe, Germany and from the Institut National Polytechnique de Grenoble, Grenoble, France, in 2003 and the Ph.D. degree from the Institut National Polytechnique de Toulouse, Toulouse, France, in 2006.

He was with the Laboratoire d'Electrotechnique de Grenoble, Grenoble, and Schneider Electric S.A., Rueil-Malmaison, where he worked on mechanical fault detection in induction machines. He is currently with Siemens AG, Munich, Germany. His research interests are fault diagnosis in electrical machines and suitable signal processing methods.

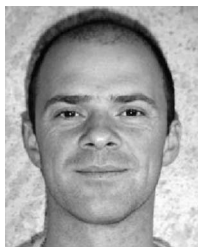

Pierre Granjon received the Ph.D. degree from the Grenoble Institute of Technology (INPG), Grenoble, France, in 2000.

In 2002, he joined the Laboratoire des Images et des Signaux (LIS). In 2007, he joined the Gipsa-Laboratory, INPG, where he is currently an Associate Professor. His research interests include signal processing applications in diagnosis and electrical engineering, such as fault diagnosis in electrical systems and power networks.

Bertrand Raison (M'03) was born in Béthune, France, in 1972. He received the M.S. and Ph.D. degrees in electrical engineering from the Institut National Polytechnique de Grenoble (INPG), Grenoble, France, in 1996 and 2000, respectively.

For one year, he was with the Faculté Polytechnique de Mons, Mons, Belgium, where he studied the effects of dispersed generation on electrical network stability. Since 2001, he has been an Associate Professor with the Laboratoire d'Electrotechnique de Grenoble, INPG. His general research interests are fault detection and localization in electrical systems (drives, converters, and electrical networks).

Gilles Rostaing was born in St. Jean de Maurienne, France, in 1966. He received the Ph.D. degree in electrical engineering from the Institut National Polytechnique de Grenoble (INPG), Grenoble, France, in 1997.

In 1997, he joined the Laboratoire d'Electrotechnique de Grenoble, INPG, where he is currently an Associate Professor. He is working on an experimental bench for bearing fault detection in induction machines. His general interests cover fault diagnosis in electrical systems.